



Synthesis of a NIR fluorescent dye and its application for rapid detection of HSO_3^- in living cells

Qiang Zhang^a, Dandan Bu^a, Haohui Ren^b, Mingming Yu^{a,*}, Hongyan Zhang^{c,**}, Zhanxian Li^{a,***}

^a Green Catalysis Center and College of Chemistry, Zhengzhou University, Zhengzhou, 450001, China

^b Key Laboratory of Photochemical Conversion and Optoelectronic Materials, Technical Institute of Physics and Chemistry, Chinese Academy of Sciences, Beijing, 100190, China

^c Beijing Key Laboratory of Clothing Materials R & D and Assessment, Beijing Engineering Research Center of Textile, Nanofiber, Beijing Institute of Fashion Technology, Beijing, 100029, China

ARTICLE INFO

Keywords:

Ratiometric fluorescent probe
NIR
 HSO_3^-
Michael addition
HeLa cells

ABSTRACT

SO_2 and its derivatives (HSO_3^- , SO_3^{2-}) play a significant important role in many industries and organisms. Based on coumarin and benzopyranose, a promising NIR ratiometric fluorescent probe BAOA (11-oxo-2,2',3,3',6,7,7',8'-octahydro-1H,1'H,5H,6'H,11H- [10,12'-bipyrano [2,3-f] pyrido [3,2,1-ij] quinolin]-13'-ium perchlorate) was designed and developed to detect HSO_3^- rapidly and sensitively. The sensing mechanism was Michael addition reaction, in which, strongly nucleophilic HSO_3^- attacked carbon-carbon double bonds and BAOA- HSO_3^- was formed. A superior linear calibration curve between the fluorescence ratio I_{490}/I_{722} and concentrations of HSO_3^- was obtained in the range of 1.25–8.75 $\mu\text{mol/L}$ and the LOD was figured out as 63.0 nmol/L. Cell experiments showed that BAOA could not only locate mitochondria, lysosomes, ER and Golgi but also detect exogenous HSO_3^- in living cells.

1. Introduction

Sulfur dioxide (SO_2) plays an extremely important role as the most common sulfur oxide. SO_2 is widely dissolved in aqueous solution to form equilibrium mixtures, which are bisulfite and sulfite ($\text{HSO}_3^-/\text{SO}_3^{2-}$, with a molar ratio of about 3:1). HSO_3^- has been widely used in many health-related industries such as food, beverages and pharmaceuticals [1–3]. However, overexpression of HSO_3^- will consume a variety of diseases, which cause atherosclerosis, essential hypertension, hypoxic pulmonary hypertension and fibrosis of the lung tissue [4–9]. Endogenous $\text{HSO}_3^-/\text{SO}_3^{2-}$ is generated from thiol-containing amino acids such as cysteine and glutathione, which play an important role in various physiological processes such as vasodilation, antioxidation and mitigation of inflammation [10–15]. Hence, it is necessary to develop excellent methods for efficient and sensitive detection of HSO_3^- .

With the development of detection technology, various methods of detecting $\text{HSO}_3^-/\text{SO}_3^{2-}$ have been discovered and reported by researchers, such as chromatography, titration analysis,

chemiluminescence, electrochemistry, enzyme technology and fluorescence, etc [16–25]. Compared with other technologies, fluorescence analysis method has overwhelming advantages of simple operation, high sensitivity, short response time, high specificity and selectivity, high spatial and temporal resolution, and can be used in vitro and biological imaging [26–31]. It has widely been considered as a promising method for the detection of small molecules. Up to now, explosive molecular fluorescent probes had been fabricated and investigated for detecting HSO_3^- . The main reaction mechanisms include nucleophilic reaction with aldehydes and nucleophilic reaction with carbon and carbon double bonds [32–34]. Among numerous types of fluorescent probes, ratiometric fluorescent probes with improved signal-to-noise ratio (SNR) have attracted wide attention because of their internal self-calibration, reducing interference from the background and improving the detection accuracy of HSO_3^- [35–40]. However, the reported probes still had some limitations, such as low fluorescence intensity and long response time. In addition, compared with fluorescent probes with short emission wavelengths, near-infrared (NIR) probes

* Corresponding author.

** Corresponding author.

*** Corresponding author.

E-mail addresses: yumm@zzu.edu.cn (M. Yu), zhyzzh@126.com (H. Zhang), lizx@zzu.edu.cn (Z. Li).

were more attractive in the wavelength range of 650–900 nm, in which biomolecules had almost no interference, the depth of sample penetration was large and it has minimal harm to biological system [41]. Therefore, it is urgent to develop NIR fluorescent dyes that can sensitively detect $\text{HSO}_3^-/\text{SO}_3^{2-}$.

Keeping these considerations in mind, herein, using 3-aminophenol as raw material, a new NIR ratiometric fluorescent probe BAOA (11-oxo-2,2',3,3',6,7,7',8'-octahydro-1H,1'H,5H,6'H,11H-[10,12'-bipyrido [2,3-f] pyrido [3,2,1-ij] quinolin]-13'-ium perchlorate) was designed and developed (ba, figures S1, S2 and S3), in which the oxygen positive ion on the benzopyran ring was a strongly electron-absorbing group, reducing the electron cloud density and making the C=C double bonds strongly electrophilic. The strong nucleophilic HSO_3^- can attack carbon-carbon double bond to form BAOA- HSO_3^- by Michael addition reaction. The sensing mechanism had been verified by nuclear magnetic titration experiments and high resolution mass spectrometry. Probe BAOA can quantitatively detect HSO_3^- in the concentration range of 1.25–8.75 $\mu\text{mol/L}$ and the LOD was calculated to be 63.0 nmol/L. Cell experiments showed that BAOA could not only locate mitochondria, lysosomes, ER and Golgi but also detect exogenous HSO_3^- in living cells. Further studies showed that probe BAOA had good selectivity and anti-interference ability toward HSO_3^- against common anions, cations and small biomolecules. Moreover, BAOA not only had good localization ability in mitochondria, lysosomes, ER and Golgi but also could detect exogenous HSO_3^- in living cells.

2. Experimental

2.1. Materials

3-Aminophenol, 2-bromo-3-chloropropane, acetoacetic ester, N,N-dimethylformamide, acetic ether, dichloromethane, anhydrous ethanol, anhydrous methanol, petroleum ether, dimethyl sulfoxide, methyl sulfonic acid, NaHCO_3 , POCl_3 , K_2CO_3 , Na_2SO_4 , NaHSO_3 , NaOH , NaF , NaCl , NaBr , NaI , KCl , CaCl_2 , AlCl_3 , ZnCl_2 , FeCl_2 , FeCl_3 , SnCl_2 , $\text{Pb}(\text{NO}_3)_2$, CuCl , CuCl_2 , MgCl_2 , AgCl , $\text{Ni}(\text{NO}_3)_2$, MnCl_2 , $\text{Co}(\text{NO}_3)_2$, $\text{Cd}(\text{NO}_3)_2$, Na_3PO_4 , Na_2HPO_4 , NaH_2PO_4 , Na_2CO_3 , NaBF_4 , NaI , NaN_3 , NaSCN , NaNO_3 , NaHSO_4 , $\text{Na}_2\text{C}_2\text{O}_4$, NaNO_2 , Ala, Arg, Asp, Cys, Gln, Glu, Gly, GSH, Hcy, His, Ile, Leu, Met, Phe, Pro, Ser, Thr, Trp, Val, H_2O_2 . All reagents and drugs were analytical grade and used without any further purification. Twice-distilled water was used throughout all the experiments.

2.2. Laboratory apparatus

Dual-beam UV-vis Spectrophotometer (TU-1901), Fluorescence spectrophotometer (F-4600), pH meter (PHS-2F), 400 M NMR spectrometer (AVIII HD 400), 600 M NMR spectrometer (AVIII HD 600), High-resolution mass spectrometer (IonSpec4.7), Rotary evaporator (RE-2000B), Electronic analytical balance (FA2004), Vacuum drying oven (DZF-6020), Constant temperature magnetic stirrer (85-2), Ultrasonic cleaner (SB-100D), Circulating water vacuum pump (SHB-3), Vacuum oil pump (2XZ-4), Digital camera (D3300), Portable UV analyzer (ZF-5).

2.3. The parameters of the solution in spectra

In Fig. S4, the solution containing 2100 μL PBS and 900 μL DMSO was chosen because it has the most excellent fluorescence change before and after adding HSO_3^- . The concentration of BAOA was 1×10^{-3} mol/L (dissolved in DMSO solution). The BAOA solution of 30 μL was removed with a liquid transfer gun and added to 3000 μL solution containing 2100 μL PBS and 900 μL DMSO ($V_{\text{PBS}}:V_{\text{DMSO}} = 7:3$), the final concentration of BAOA in the test system was 1×10^{-5} mol/L.

The concentrations of anion ions, metal ions and small biomolecules used in the detection were 0.01 mol/L initially. The concentration of HSO_3^- was 0.0025 mol/L.

2.4. Synthesis of B1

3-aminophenol (2.05 g, 18.785 mmol), NaHCO_3 (6.3125 g, 75.14 mmol) and 1-bromo-3-chloropropane (11.83 g, 75.14 mmol) were added to a 100 mL round bottom flask and were evenly dissolved in DMF (30 mL). Then the reaction mixture was stirred at 70 °C for 12 h until the reaction was completed. After cooling to room temperature, the reaction solution was poured into ice water. The solution was extracted with ethyl acetate, and then washed with water. The remaining solution was dried by Na_2SO_4 and further purified by silica gel column chromatography (PE: EA = 20 : 1, v/v) to get white solid B1 (900 mg, yield: 25.3%). ^1H NMR (600 MHz, $\text{DMSO}-d_6$) δ 8.63 (s, 1H), 6.48 (d, $J = 8.0$ Hz, 1H), 6.00 (d, $J = 8.0$ Hz, 1H), 3.03–2.97 (m, 4H), 2.57 (t, $J = 6.5$ Hz, 2H), 2.51 (d, $J = 6.3$ Hz, 2H), 1.86–1.80 (m, 4H). ^{13}C NMR (151 MHz, $\text{DMSO}-d_6$) δ 153.0, 143.6, 126.0, 112.0, 107.7, 103.0, 49.6, 49.1, 26.7, 22.1, 21.4, 21.0.

2.5. Synthesis of B2

2 mL of dried DMF was placed in a round neck flask and stirred in an ice-water bath for 15 min. Then 0.5 mL of POCl_3 was added dropwise to the flask and stirring for 30 min. The product B1 (189.2 mg, 1 mmol) from the previous step dissolved in DMF was added dropwise to the reaction system and stirred at room temperature for 1 h. Then, the temperature was raised to 100 °C for 1 h and the heating was stopped. After cooling to room temperature, 10 mL of water was added to the reaction flask while the pH of the reaction system was adjusted to 6–8 with saturated potassium carbonate solution, and stirring was continued for 1 h. After the reaction was completed, it was extracted with CH_2Cl_2 , and then the organic phase was washed with saturated brine, and dried overnight with anhydrous sodium sulfate. After silica gel column chromatography, a light yellow solid product was obtained. (154 mg, yield: 70.9%). ^1H NMR (600 MHz, $\text{DMSO}-d_6$) δ 11.85 (s, 1H), 9.36 (s, 1H), 6.98 (s, 1H), 3.28 (dd, $J = 12.2, 7.3$ Hz, 4H), 2.62 (t, $J = 6.2$ Hz, 2H), 2.54 (t, $J = 6.4$ Hz, 2H), 1.83 (dd, $J = 12.1, 6.1$ Hz, 4H). ^{13}C NMR (151 MHz, $\text{DMSO}-d_6$) δ 191.6, 158.4, 149.2, 130.9, 113.4, 110.0, 104.2, 49.5, 49.0, 26.5, 21.0, 19.9, 19.2.

2.6. Synthesis of B3

B2 (217 mg, 1 mmol) was dissolved in 5 mL of absolute ethanol, and ethyl acetate (260 mg, 2 mmol) and piperidine (80 μL , 0.81 mmol) were added to the reaction solution. Under the protection of argon, it was heated to reflux for 5 h and then cooled to room temperature. Filtered with suction and washed with *n*-hexane to obtain an orange solid (205.6 mg, yield: 72.6%). ^1H NMR (600 MHz, CDCl_3) δ 8.33 (s, 1H), 6.96 (s, 1H), 3.34 (dd, $J = 12.0, 6.5$ Hz, 4H), 2.88 (t, $J = 6.4$ Hz, 2H), 2.76 (t, $J = 6.2$ Hz, 2H), 2.67 (s, 3H), 2.01–1.94 (m, 4H). ^{13}C NMR (151 MHz, CDCl_3) δ 196.0, 161.2, 153.8, 148.8, 147.8, 127.8, 114.9, 108.1, 105.6, 50.4, 50.0, 30.6, 27.4, 21.2, 20.2, 20.1.

2.7. Synthesis of BAOA

B3 (283.4 mg, 1 mmol) and B2 (260.4 mg, 1.2 mmol) were dissolved in methyl sulfonic acid and stirred at 90 °C for 6 h. After the reaction was cooled to room temperature, the reaction droplets were added to the ice salt water to form precipitate, the precipitate was filtered and washed with water, and the crude product was separated by silica gel column chromatography to obtain blue and black solid (220 mg, yield: 47.3%). ^1H NMR (400 MHz, CDCl_3) δ 8.54 (s, 1H), 8.25 (d, $J = 8.3$ Hz, 1H), 8.17 (d, $J = 8.4$ Hz, 1H), 7.39 (d, $J = 16.9$ Hz, 2H), 3.72–3.61 (m, 4H), 3.47 (dd, $J = 10.1, 5.3$ Hz, 4H), 3.16 (t, $J = 5.8$ Hz, 2H), 2.93–2.81 (m, 6H), 2.16 (d, $J = 27.5$ Hz, 8H). ^{13}C NMR (101 MHz, CDCl_3) δ 162.0, 158.7, 153.4, 153.0, 152.2, 150.8, 145.1, 143.8, 129.0, 127.4, 127.3, 121.4, 117.9, 110.3, 109.9, 105.8, 105.4, 104.9, 51.3, 51.0, 50.4, 27.7, 27.3, 27.2, 20.9, 20.3, 19.9, 19.8, 19.4.

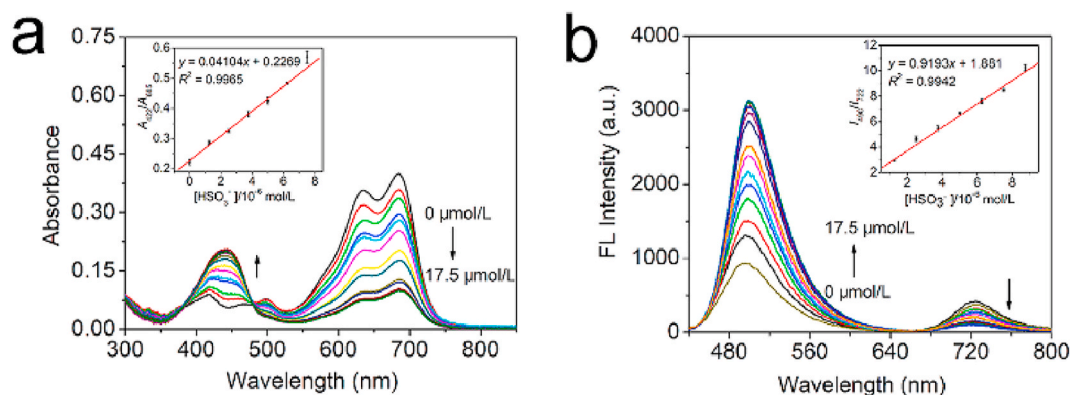


Fig. 1. (a) UV-vis spectral changes of 1×10^{-5} mol/L BAOA with various concentrations of HSO_3^- (0–17.5 $\mu\text{mol/L}$) in PBS buffered aqueous solution ($V_{\text{PBS}}:V_{\text{DMSO}} = 7:3$, $\text{pH} = 7.4$); inset: Linear plot of the ratio A_{422}/A_{685} against HSO_3^- concentrations in the range 0–7.5 $\mu\text{mol/L}$. (b) Fluorescence spectral changes of 1×10^{-5} mol/L BAOA with various concentrations of HSO_3^- (0–17.5 $\mu\text{mol/L}$) in PBS buffered aqueous solution ($V_{\text{PBS}}:V_{\text{DMSO}} = 7:3$, $\text{pH} = 7.4$); inset: Linear plot of the ratio I_{490}/I_{722} against HSO_3^- concentrations in the range 1.25–8.75 $\mu\text{mol/L}$.

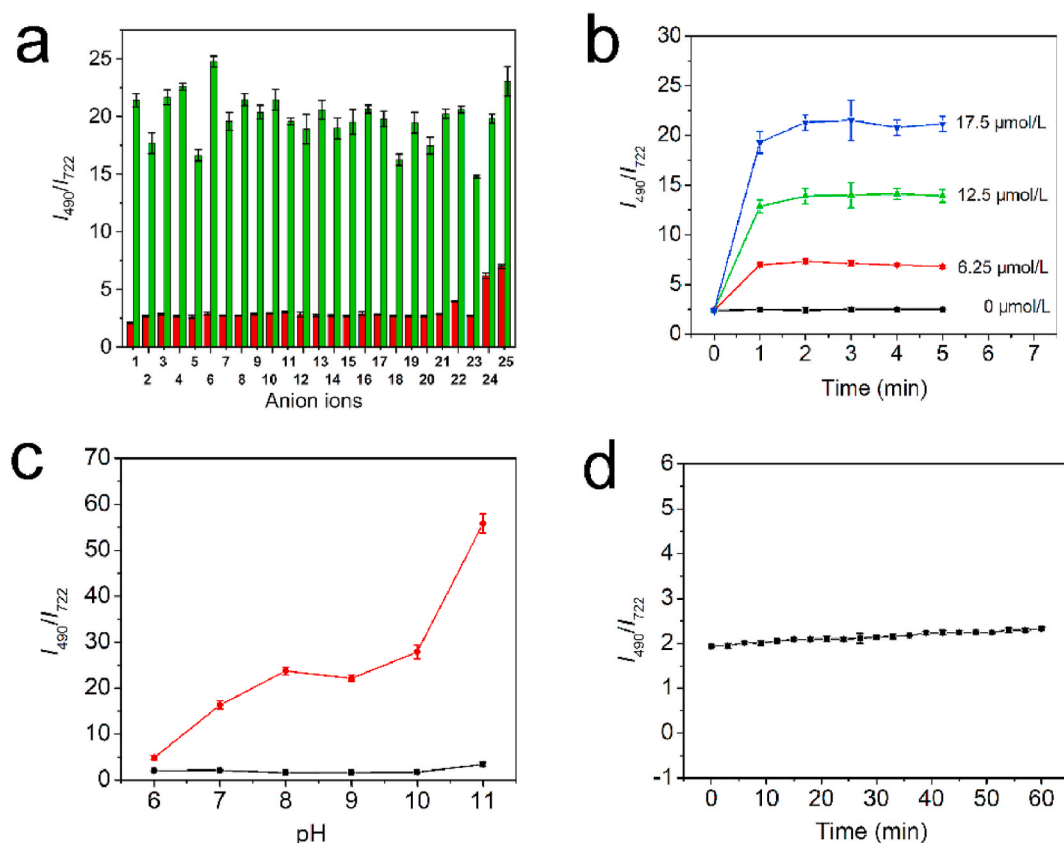


Fig. 2. (a) Emission spectral responses of BAOA solution ($V_{\text{PBS}}:V_{\text{DMSO}} = 7:3$, 1×10^{-5} mol/L) with different anions ions at I_{490}/I_{722} (red bars) and the ratio of BAOA for HSO_3^- (17.5 $\mu\text{mol/L}$) at I_{490}/I_{722} in the presence of anions ions (17.5 $\mu\text{mol/L}$) (green bars) ($\lambda_{\text{ex}} = 425$ nm). Numbers 1–25 represent Blank, F^- , Cl^- , Br^- , I^- , PO_4^{3-} , HPO_4^{2-} , H_2PO_4^- , CO_3^{2-} , HCO_3^- , SO_4^{2-} , HSO_4^- , N_3^- , NO_2^- , NO_3^- , BrO_3^- , BF_4^- , $\text{C}_2\text{O}_4^{2-}$, SCN^- , SiO_3^{2-} , $\text{S}_2\text{O}_3^{2-}$, ClO^- , $\text{P}_2\text{O}_7^{4-}$, H_2S and S^{2-} respectively. (b) Real-time records of fluorescence emission ratio I_{490}/I_{722} changes of BAOA with different concentrations of HSO_3^- (0, 6.25, 12.5, 17.5 $\mu\text{mol/L}$). (c) Fluorescence intensity ratio I_{490}/I_{722} of BAOA ($V_{\text{PBS}}:V_{\text{DMSO}} = 7:3$, 1×10^{-5} mol/L) in the absence (black) and presence (red) of HSO_3^- (17.5 $\mu\text{mol/L}$) under pH values of 6–11. (d) Fluorescence intensity ratio I_{490}/I_{722} of BAOA ($V_{\text{PBS}}:V_{\text{DMSO}} = 7:3$, 1×10^{-5} mol/L) as irradiation time changing ($\lambda_{\text{ex}} = 425$ nm).

3. Results and discussion

To further investigate the response ability of BAOA to HSO_3^- , UV-vis absorption spectra were performed. As shown in Fig. 1a, with the increasing HSO_3^- concentration, absorbance at 422 nm (A_{422}) was increasing while that at 685 nm (A_{685}) was declining gradually. Insert of Fig. 1a proved that BAOA had a linear calibration curve between A_{422}/A_{685} and the HSO_3^- concentration in the range of 0–7.5 $\mu\text{mol/L}$ ($R^2 =$

0.9965). Fig. 1b explored the fluorescence sensing properties of BAOA for HSO_3^- . The fluorescence intensity at 490 nm (I_{490}) was significantly enhanced with the increase of HSO_3^- concentration at 425 nm excitation, but that at 722 nm (I_{722}) decreased. A linear calibration curve was obtained between the fluorescence intensity ratio I_{490}/I_{722} and HSO_3^- concentration in the range of 1.25–8.75 $\mu\text{mol/L}$ ($R^2 = 0.9942$) (The inset of Fig. 1b). A minimum detection limit was calculated to be 63.0 nmol/L [42]. The above studies showed that the synthesized BAOA can be used

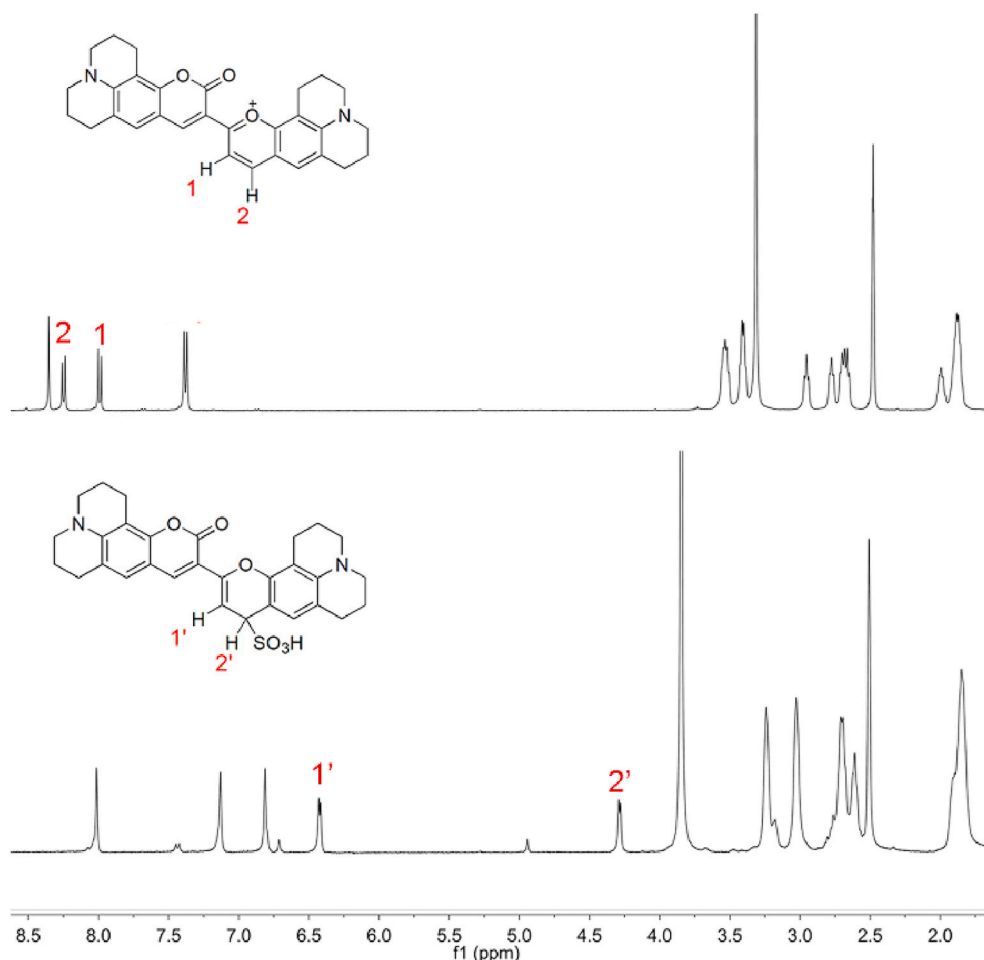


Fig. 3. ¹H NMR titration spectra of probe BAOA without and with 2.0 eq. of HSO₃⁻ in DMSO-*d*₆.

as a ratiometric fluorescent probe for quantitative detection of HSO₃⁻. In Table S1, obvious wavelength changes, Stokes shift and molar extinction coefficient were observed, indicating that BAOA had a better response to HSO₃⁻.

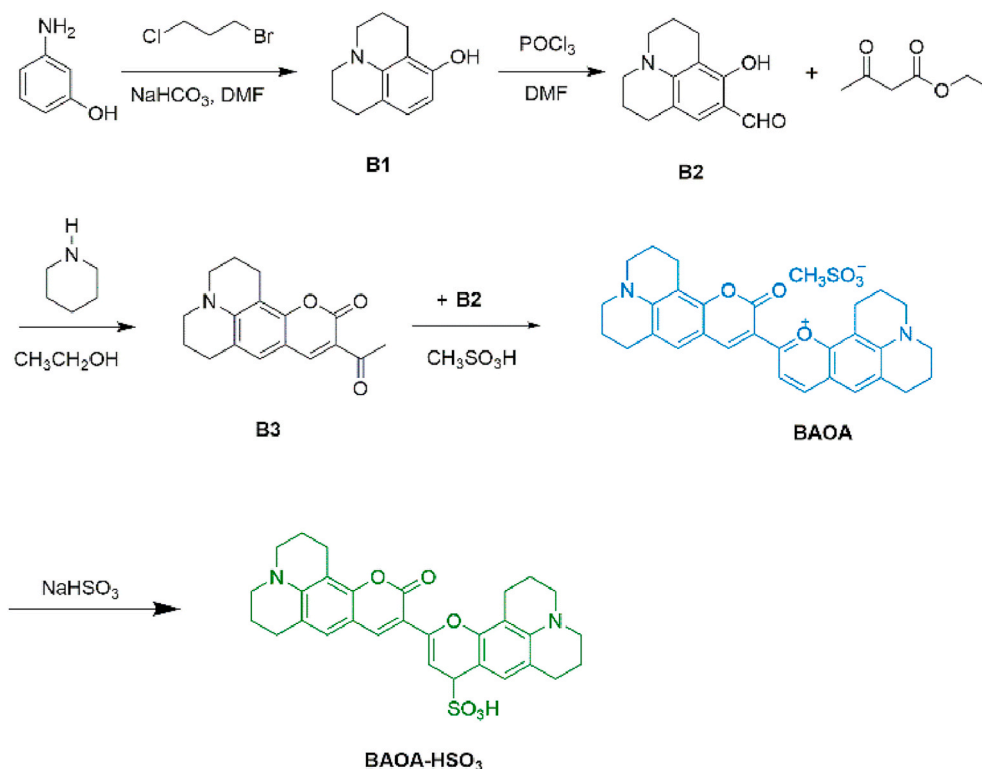
The changes in the fluorescence emission spectra were studied to determine whether BAOA was specific to HSO₃⁻. As indicated in the red bars of Fig. 2a, the selected anions only didn't cause significant changes in the fluorescence intensity ratio I₄₉₀/I₇₂₂. The fluorescence intensity ratio I₄₉₀/I₇₂₂ increased obviously only after adding HSO₃⁻, which indicated that BAOA has good selectivity toward HSO₃⁻. In the mixture of probe BAOA and the mentioned anions, addition of HSO₃⁻ could increase the fluorescence intensity ratio I₄₉₀/I₇₂₂ (green bars of Fig. 2a), indicating that the above anions didn't interfere with the detection of HSO₃⁻. As shown in Table S1, absorption wavelength changes from 685 nm to 422 nm and excitation wavelength changes from 722 nm to 490 nm. Molar extinction coefficients have changed greatly before and after reaction with HSO₃⁻ (ε₄₂₂ changes from 8500 L mol⁻¹ cm⁻¹ to 17,600 L mol⁻¹ cm⁻¹, ε₆₈₅ changes from 40,000 L mol⁻¹ cm⁻¹ to 10,000 L mol⁻¹ cm⁻¹). As mentioned in Fig. S5, similar results were obtained as for the mentioned metal ions and small biomolecules. Thereby, BAOA can specifically detect HSO₃⁻.

Dynamics of BAOA to detect HSO₃⁻ was investigated in Fig. 2b. BAOA and HSO₃⁻ can react completely in about 1 min, which indicated that BAOA could quickly response to HSO₃⁻. The fluorescence response of BAOA to HSO₃⁻ at different pH values was discussed in Fig. 2c. The fluorescence intensity ratio (I₄₉₀/I₇₂₂) of BAOA was constant in the range of 6–11. When HSO₃⁻ was added to the test system, I₄₉₀/I₇₂₂ increased sharply in the range of 7–11. Therefore, BAOA can be used to

detect HSO₃⁻ in an extensive range of pH values. In Fig. 2d, I₄₉₀/I₇₂₂ of BAOA solution basically unchanged during 1 h of irradiation time indicating that BAOA had good photostability.

¹H NMR titration experiments (Fig. 3) and high resolution mass spectrometry analysis (Fig. S6) were carried out to explore the response mechanism of BAOA toward HSO₃⁻. The sensing mechanism based on Michael addition reaction was proposed (Scheme 1) [43]. The ¹H NMR titration spectra showed that the peaks at the chemical shifts of 8.05 ppm (H1) and 8.30 ppm (H2) of BAOA gradually disappeared and two new peaks appeared in the high field region, which were 6.45 ppm (H1') and 4.28 ppm (H2'). The movement of the two hydrogenated displacement signals was consistent with ¹H NMR of the putative response mechanism. The mass spectrum peak of *m/z* = 547.1902 (Fig. S6) was consistent with the hydrogenation ion peak of the speculative product (C₃₀H₃₀N₂O₆S, *m/z* = 547.1897), which further proved that the inferred response mechanism was correct. Compared with the reported fluorescent probes toward HSO₃⁻ (Table 1), probe BAOA has shorter response time, lower LOD, and could be used as a NIR ratiometric fluorescence probe.

To explore the localization ability of probe BAOA, the co-localization experiments of commercial dye Mito-Tracker deep-red, lyso-Tracker deep red, ER-Tracker Red and Golgi-Tracker Red with BAOA were carried out, respectively. As shown in Fig. 4, the Pearson co-localization coefficient of the mitochondrial co-localization experiment was calculated as 0.762. Similar to the result, the Pearson co-localization coefficient of lysosomal, ER and Golgi co-localization was 0.864, 0.877 and 0.940, respectively. According to the above data, BAOA could serve as mitochondrial, lysosomal, ER and Golgi localization tracker. Moreover,



Scheme 1. Synthetic route of BAOA and its detection mechanism toward HSO_3^- (The anion of BAOA was CH_3SO_3^-).

Table 1

Comparison of this work with previously reported methods for HSO_3^- detection.

probe	Detection mode	Detection condition	Response time	LOD	Linear ranges	Ref
Probe 1	On-off	PBS solution	30 min	0.46 μM	0–200 μM	[42]
probe 2	On-off	PBS/DMSO	10 min	2.01 μM	0–150 μM	[43]
ASHTI	On-off	PBS/DMSO	15 min	0.27 μM	0.8–60 μM	[44]
L2	Off-on	PBS/DMSO	13 min	0.59 μM	0–9 μM	[45]
L	On-off	HEPES solution	Not mention	0.45 μM	1–13 μM	[46]
BAOA	Ratiometric	PBS/DMSO	1 min	63.0 nM	1.25–8.75 μM	This work

the toxicity experiment of BAOA on HeLa cells was carried out. As shown in Table S2, when the concentration of BAOA was 10 $\mu\text{mol/L}$, the cell survival rate was as high as 0.826, showing low toxicity of BAOA.

To explore the potential applications of BAOA toward exogenous HSO_3^- in living cells, cell experiments were characterized. The fluorescence imaging results were shown in Fig. 5, which exhibited weak green fluorescence after co-incubating with HeLa cells. The green fluorescence was enhanced by further incubation containing BAOA and HSO_3^- . The morphology of HeLa cells in the bright field images didn't change remarkably, indicating that HeLa cells still survived. These phenomena suggested that BAOA had membrane permeability and could be capable of detecting exogenous HSO_3^- in HeLa cells.

4. Conclusion

The NIR ratiometric fluorescent probe BAOA was synthesized by four-step reaction based on coumarin and benzopyranose. BAOA can quantitatively detect HSO_3^- in the range of 1.25–8.75 $\mu\text{mol/L}$ via

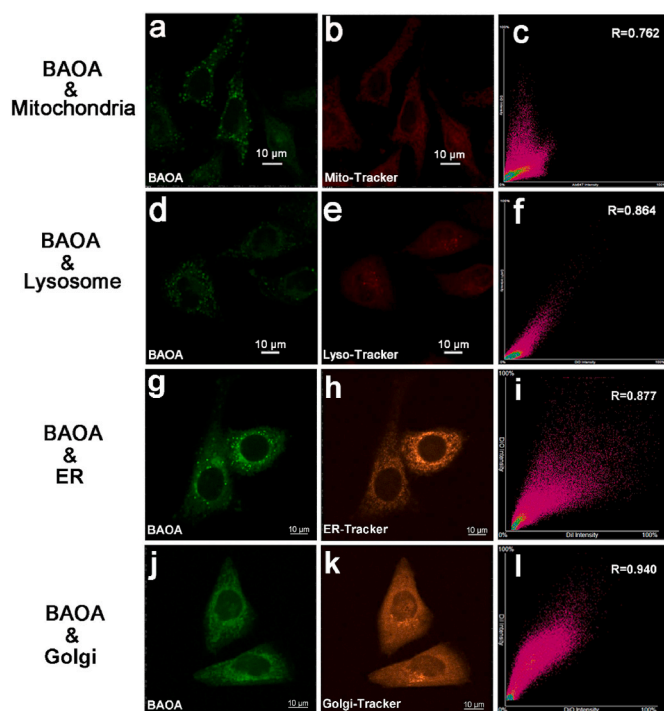


Fig. 4. (a) (d) (g) (j) Fluorescence photo of the green channel of BAOA (10 μM) in HeLa cells. (b) (e) Fluorescence photo of the red channel of Mito-Tracker Deep Red (10 μM) and lyso-Tracker deep red (10 μM) in HeLa cells. (h) (k) Fluorescence photo of the orange channel of ER-Tracker Red (10 μM) and Golgi-Tracker Red (10 μM) in HeLa cells. (c) (f) (i) (l) Intensity correlation plot of BAOA and Mito Tracker Deep Red, lyso-Tracker deep red, ER-Tracker Red and Golgi-Tracker Red.

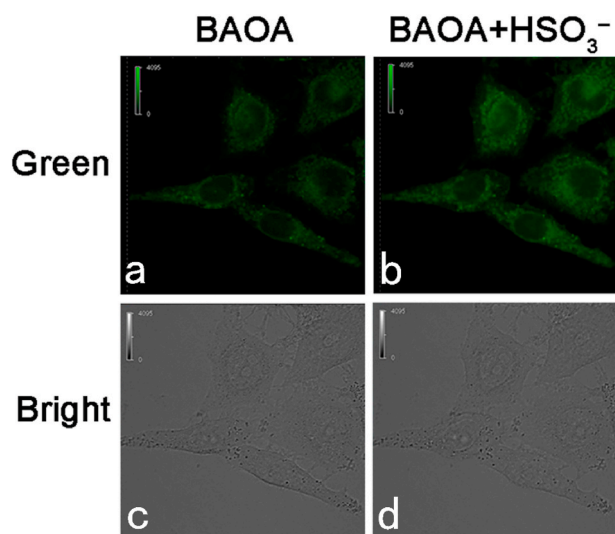


Fig. 5. (a) Fluorescence image of the green channel of BAOA (10 μM) in HeLa cells after incubating 30 min and (c) Bright-field image; (b) Fluorescence image of the green channel of BAOA (10 μM) and HSO_3^- (17.5 μM) in HeLa cells and (d) Bright-field image.

ratiometric fluorescence method and the LOD was 63.0 nmol/L. Moreover, BAOA not only recognized HSO_3^- in a wide range of pH values (7–11), but also could detect HSO_3^- in short response time (1 min). The mechanism of BAOA toward HSO_3^- was proved to be Michael addition reaction. Cell experiments showed that BAOA had the ability to localize mitochondria, lysosomes, ER and Golgi and could also detect HSO_3^- in living cells.

CRedit authorship contribution statement

Qiang Zhang: Writing – original draft. **Dandan Bu:** Data curation. **Haohui Ren:** Visualization. **Mingming Yu:** Conceptualization, Writing – review & editing. **Hongyan Zhang:** Software, Validation. **Zhanxian Li:** Supervision, Funding acquisition.

Declaration of competing interest

The authors declare that they have no known competing financial interests or personal relationships that could have appeared to influence the work reported in this paper.

Acknowledgements

This study was supported by the financial supports from National Natural Science Foundation of China (U1704161, U1504203, 21601158), and Zhengzhou University (32210431).

Appendix A. Supplementary data

Supplementary data to this article can be found online at <https://doi.org/10.1016/j.dyepig.2021.109753>.

References

- [1] Finkel T, Holbrook NJ. Oxidants, oxidative stress and the biology of ageing. *Nature* 2000;408:239–47.
- [2] Rabinowitz JD, White E. Autophagy and metabolism. *Science* 2010;330:1344–8.
- [3] Zhong K, Chen L, Yan X, Tang Y, Hou S, Li X, Tang L. Dual-functional multi-application probe: rapid detection of H_2S and colorimetric recognition of HSO_3^- in food and cell. *Dyes Pigments* 2020;182:108656.
- [4] Ren H-X, Huo F-J, Wu X, Liu X-G, Yin C-X. An ESIPt-induced NIR fluorescent probe to visualize mitochondrial sulfur dioxide during oxidative stress in vivo. *Chem Commun* 2021;57:655–8.

- [5] Zhou R, Niu L, Hu Y, Qi Q, Huang W, Yang L. A novel dual-function fluorescent probe for the rapid detection of bisulfite and hydrogen peroxide in aqueous solution and living cells. *Spectrochim Acta A* 2021;248:119226.
- [6] Zhang W-J, Huo F-J, Cheng F-Q, Yin C-X. Employing an ICT-FRET integration platform for the real-time tracking of SO_2 metabolism in cancer cells and tumor models. *J Am Chem Soc* 2020;142:6324–31.
- [7] Singha S, Jun YW, Sarkar S, Ahn KH. An endeavor in the reaction-based approach to fluorescent probes for biorelevant analytes: challenges and achievements. *Acc Chem Res* 2019;52:2571–81.
- [8] Huang Y-F, Zhang Y-B, Huo F-J, Chao J-B, Cheng F-Q, Yin C-X. A new strategy: distinguishable multi-substance detection, multiple pathway tracing based on a new site constructed by the reaction process and its tumor targeting. *J Am Chem Soc* 2020;142:18706–14.
- [9] Xu J, Pan J, Jiang X, Qin C, Zeng L, Zhang H, Zhang JF. A mitochondria-targeted ratiometric fluorescent probe for rapid, sensitive and specific detection of biological SO_2 derivatives in living cells. *Biosens Bioelectron* 2016;77:725–32.
- [10] Zhang W, Liu T, Huo F, Ning P, Meng X, Yin C. Reversible ratiometric fluorescent probe for sensing bisulfate/ H_2O_2 and its application in zebrafish. *Anal Chem* 2017;89:8079–83.
- [11] Li D-P, Wang Z-Y, Su H, Miao J-Y, Zhao B-X. Fluorescence detection of endogenous bisulfite in liver cancer cells using an effective ESIPt enhanced FRET platform. *Chem Commun* 2017;53:577–80.
- [12] Duan C, Zhang J-F, Hu Y, Zeng L, Su D, Bao G-M. A distinctive near-infrared fluorescence turn-on probe for rapid, sensitive and chromogenic detection of sulfite in food. *Dyes Pigments* 2019;162:459–65.
- [13] Yue Y-K, Huo F-J, Ning P, Zhang Y-B, Chao J-B, Meng X-M, Yin C-X. Dual-site fluorescent probe for visualizing the metabolism of Cys in living cells. *J Am Chem Soc* 2017;139:3181–5.
- [14] Liu W, Zhang D, Ni B, Li J, Weng H, Ye Y. Mitochondria-targeted and FRET based ratiometric fluorescent probe for SO_2 and its cell imaging. *Sensor Actuator B Chem* 2019;284:330–6.
- [15] Li T, Yin C, Chao J, Zhang W, Huo F. An ultra-fast, NIR, mitochondria-targeted fluorescent probe for sulfur dioxide based on benzopyrylium and its imaging of in living cells. *Sensor Actuator B Chem* 2020;305:127336.
- [16] Wang W, Li N, Liu J-T, Miao J-Y, Zhao B-X, Lin Z-M. A new FRET-based ratiometric fluorescent probe for the detection of SO_2 derivatives in mitochondria of living cells. *Dyes Pigments* 2020;181:108639.
- [17] Ma S, Wang K, Yu X, Zhang Y, Xing M, Wu X, Cao D, Liu Z. Photophysical properties and bisulfite recognition of a coumarin cyanopyridine derivative. *Dyes Pigments* 2020;182:108691.
- [18] Jiang Q, Wang Z, Li M, Song J, Yang Y, Xu X, Xu H, Wang S. A novel nopinone-based colorimetric and ratiometric fluorescent probe for detection of bisulfite and its application in food and living cells. *Dyes Pigments* 2019;171:107702.
- [19] Zhang C, Han L, Liu Q, Liu M, Gu B, Shen Y. A colorimetric and far-red fluorescent probe for rapid detection of bisulfite/sulfite in full water-soluble based on biquinolinium and its applications. *Spectrochim Acta A* 2021;253:119561.
- [20] Ci Q, Qin X, Liu J, Wang R, Li Z, Qin W, Lim K-L, Zhang C-W, Li L. Mitochondria-targeted polydopamine nanoprobe for visualizing endogenous sulfur dioxide derivatives in a rat epilepsy model. *Chem Commun* 2020;56:11823–6.
- [21] Wang R, Wang R, Ju D, Lu W, Jiang C, Shan X, Chen Q, Sun G. "ON-OFF-ON" fluorescent probes based on nitrogen-doped carbon dots for hypochlorite and bisulfite detection in living cells. *Analyst* 2018;143:5834–40.
- [22] Zhu J-L, Xu Z, Yang Y, Xu L. Small-molecule fluorescent probes for specific detection and imaging of chemical species inside lysosomes. *Chem Commun* 2019;55:6629–71.
- [23] Lan J-S, Zeng R-F, Ding Y, Zhang Y, Zhang T, Wu T. A simple pyrene-hemicyanine fluorescent probe for colorimetric and ratiometric detection of SO_2 derivatives in the mitochondria of living cells and zebrafish in vivo. *Sensor Actuator B Chem* 2018;268:328–37.
- [24] Zhong K, Chen L, Yan X, Tang Y, Hou S, Li X, Tang L. Dual-functional multi-application probe: rapid detection of H_2S and colorimetric recognition of HSO_3^- in food and cell. *Dyes Pigments* 2020;182:108656.
- [25] Han X, Zhai Z, Yang X, Zhang D, Tang J, Zhu J, Zhu X, Ye Y. A FRET-based ratiometric fluorescent probe to detect cysteine metabolism in mitochondria. *Org Biomol Chem* 2020;18:1487–92.
- [26] Li J-Z, Sun Y-H, Wang C-Y, Guo Z-Q, Shen Y-J, Zhu W-H. AND-logic based fluorescent probe for selective detection of lysosomal bisulfite in living cells. *Anal Chem* 2019;91:11946–51.
- [27] Pan X, Cheng S, Zhang C, Qi X. Two highly sensitive fluorescent probes based on cinnamaldehyde with large Stokes shift for sensing of HSO_3^- in pure water and living cells. *Anal Bioanal Chem* 2020;412:6959–68.
- [28] Tamima U, Santra M, Song CW, Reo YJ, Ahn KH. A benzopyronin-based two-photon fluorescent probe for ratiometric imaging of lysosomal bisulfite with complete spectral separation. *Anal Chem* 2019;91:10779–85.
- [29] Wang K-P, Lei Y, Sun Y, Zhang Q, Chen S, Zhang Q, Hu H-Y, Hu Z-Q. Tetrahydro[5] helicene-based fluorescent probe for rapid and sensitive detection of bisulfite in living cells. *Sensor Actuator B Chem* 2018;273:1487–94.
- [30] Ma W, Du J, Yin J, Fan J, Long S, Peng X. Quantitative recognition and ratiometric cell imaging of HSO_3^- inspired of confined-space based FRET system within human serum albumin. *Sensor Actuator B Chem* 2018;267:104–10.
- [31] Su S, Zheng Z, Zhang Q-L, Ni X-L. Fatty-chain-switched cationic fluorescent probe for SCN^- , PF_6^- , and HSO_3^- recognition in water: study of anion selectivity and sensitivity. *Dyes Pigments* 2021;185:108903.
- [32] Paul S, Ghoshal K, Bhattacharyya M, Maiti DK. Detection of HSO_3^- : a rapid colorimetric and fluorimetric selective sensor for detecting biological SO_2 in food and living cells. *ACS Omega* 2017;2:8633–9.

- [33] Ma S, Wang K, Yu X, Zhang Y, Xing M, Wu X, Cao D, Liu Z. Photophysical properties and bisulfite recognition of a coumarin cyanopyridine derivative. *Dyes Pigments* 2020;182:108691.
- [34] Yu T, Yin G, Niu T, Yin P, Li H, Zhang Y, Chen H, Zeng Y, Yao S. A novel colorimetric and fluorescent probe for simultaneous detection of $\text{SO}_3^{2-}/\text{HSO}_3^-$ and HSO_4^- by different emission channels and its bioimaging in living cells. *Talanta* 2018;176:1–7.
- [35] Ye Z, Duan C, Sheng R, Xu J, Wang H, Zeng L. A novel colorimetric and ratiometric fluorescent probe for visualizing SO_2 derivatives in environment and living cells. *Talanta* 2018;176:389–96.
- [36] Chao J, Wang X, Liu Y, Zhang Y, Huo F, Yin C, Zhao M, Sun J, Xu M. A pyrene-thiophene based fluorescent probe for ratiometric sensing of bisulfite and its application in vivo imaging. *Sensor Actuator B Chem* 2018;272:195–202.
- [37] Yang S, Wen X, Yang X, Li Y, Guo C, Zhou Y, Li H, Yang R. Visualizing endogenous sulfur dioxide derivatives in febrile-seizure-induced hippocampal damage by a two-photon energy transfer cassette. *Anal Chem* 2018;90:14514–20.
- [38] Bi K, Tan R, Hao R, Miao L, He Y, Wu X, Zhang J, Xu R. A carbazole-hemicyanine dye based ratiometric fluorescent probe for selective detection of bisulfite (HSO_3^-) in cells and *C. elegans*. *Chin Chem Lett* 2019;30:545–8.
- [39] Wu L, Qi S, Liu Y, Wang X, Zhu L, Yang Q, Du J, Xu H, Li Y. A novel ratiometric fluorescent probe for differential detection of HSO_3^- and ClO^- and application in cell imaging and tumor recognition. *Anal Bioanal Chem* 2021;413:1137–48.
- [40] Yan YH, Wu QR, Che QL, Ding MM, Xu M, Miao JY, Zhao BX, Lin ZM. A mitochondria-targeted fluorescent probe for the detection of endogenous SO_2 derivatives in living cells. *Analyst* 2020;145:2937–44.
- [41] Li D-P, Han X-J, Yan Z-Q, Cui Y, Miao J-Y, Zhao B-X. A far-red ratiometric fluorescent probe for SO_2 derivatives based on the ESIPt enhanced FRET platform with improved performance. *Dyes Pigments* 2018;151:95–101.
- [42] Li Y, Ban Y, Wang R, Wang Z, Li Z, Fang C, Yu M. FRET-based ratiometric fluorescent detection of arginine in mitochondrion with a hybrid nanoprobe. *Chin Chem Lett* 2020;31:443–6.
- [43] Zhang W, Huo F, Cheng F, Yin C. Employing an ICT-FRET integration platform for the real-time tracking of SO_2 metabolism in cancer cells and tumor models. *J Am Chem Soc* 2020;142:6324–31.
- [44] Zeng R-F, Lan J-S, Wu T, Liu L, Liu Y, Ho R-J, Ding Y, Zhang T. A novel mitochondria-targeted near-infrared fluorescent probe for selective and colorimetric detection of sulfite and its application in vitro and vivo. *Food Chem* 2020;318:126358.
- [45] Zhang L, Wang L, Zhang X, Zhu ZJ. A colorimetric and fluorescent probe for sulfite/bisulfite based on conjugated benzothiazole derivative and imaging application in living cells. *J Photochem Photobiol Chem* 2020;395:112498.
- [46] Zou L, Xu JK, Liu X, Zhang XX, Gao YZ, Zhang G, Duan XM. A colorimetric-fluorescent HSO_3^- sensor with high-selectivity enables rapid screening and accurate analysis of environmental samples. *Microchem J* 2020;153:104461.